





Research article

Internal polymerization of epoxy group of epoxidized natural rubber by ferric chloride filled with carbon nanotubes: Mechanical, morphological, thermal and electrical properties of rubber vulcanizates

Kriengsak Damampai¹, Skulrat Pichaiyut¹, Amit Das², Charoen Nakason^{1*}

¹Faculty of Science and Industrial Technology, Prince of Songkla University, 84000 Surat Thani Campus, Thailand

²Leibniz-Institut für Polymerforschung Dresden e.V., D-01069 Dresden, Germany

Received 9 February 2022; accepted in revised form 6 April 2022

Abstract. In this work, the crosslinking reaction of epoxidized natural rubber (50 mol% epoxy, ENR-50) by metal ion namely ferric ion (Fe^{3+} , FeCl_3 , ferric chloride) was studied. It was found that a direct interaction of the ferric ion with the epoxy group as well as internal polymerization enable the ENR to be efficiently cured. The vulcanizing ENR- FeCl_3 compound was then reinforced by carbon nanotubes (CNTs). The FTIR spectra of ENR- FeCl_3 compounds without and with CNTs show the absorption peak at the wavenumber 470 cm^{-1} , which represents the $-\text{O}-\text{Fe}-\text{O}-$ linkages from a reaction of FeCl_3 and opened oxirane ring products of ENR molecules. Furthermore, the ENR- FeCl_3 compounds show a typical marching curing curve with a steady increase in torque as increasing of the testing time; especially the effect is more pronounced in CNTs filled system. Furthermore, an increase in the concentration of CNTs causes increasing in torque difference and enhancement of the mechanical properties (*i.e.*, 100% moduli and tensile strength). The SEM micrograph shows good compatibility between CNTs and the rubber matrix in the ENR- FeCl_3 compounds. Also, the electrical conductivities of ENR- FeCl_3 /CNTs nanocomposite increases with the increase of CNTs loading. It is also observed that the degradation temperature (T_d) of ENR- FeCl_3 /CNTs is shifted toward a higher temperature range with the increase of the CNTs loadings.

Keywords: nanocomposites, epoxidized natural rubber, ferric chloride, carbon nanotube, internal polymerization

1. Introduction

Natural rubber (NR) is an agricultural product which can be obtained from renewable resources and also biodegradable. Typically, NR exhibits many excellent properties, including mechanical, dynamic properties and elasticity, but its weathering and oil-resistant property are rather poor. To improve mechanical properties, electrical conductivity and other related properties of NR, various conductive fillers are normally incorporated in the compounding formulation of NR [1, 2]. Also, the modified NR like epoxidized natural rubber (ENR) [3], maleated natural rubber [4] and NR grafted with polar monomers [5], have

also been exploited to improve some important properties of NR. Currently, natural rubber nanocomposites have also been prepared by incorporating different types of nanofillers, including carbon nanotubes [6], graphene [7], and conductive carbon black [8]. Furthermore, ceramic fillers, such as barium titanate (BaTiO_3) and lead titanate (PbTiO_3) were also investigated [9]. It was found that the gum ENR and ENR/ BaTiO_3 composites exhibit higher mechanical properties and electrical conductivities than those of the gum NR and NR/ PbTiO_3 composites. This is attributed to the higher polarity of ENR than the unmodified NR, which makes them enable to promote the

*Corresponding author, e-mail: charoen.nakason@gmail.com

© BME-PT

interactions between functional groups of ENR and at the ceramic filler surfaces [9].

Vulcanization of rubber is of important process in the manufacturing of high-quality rubber products for various industrial and commodity applications. Typically, a sulfur vulcanization system has been used to cure natural rubber and its modified form, such as ENR and maleated Natural rubber (MNR). Other commonly used vulcanization systems are peroxide, phenolic, and metal oxide vulcanization systems, together with radiation vulcanization and metal ions [10]. Generally, metal ions have been used as an additive to tailor various properties of rubber. For instance, some transition metal ions (*i.e.*, Mn^{2+} , Cu^{2+} and Fe^{2+}) have been found to accelerate the oxidative degradation of the solid rubber via fragmentation of the polyisoprene chains [11]. Also, the presence of divalent metal ions, such as Cu^{2+} , Fe^{2+} and Zn^{2+} causes a delay in the maturation time in the pre-vulcanized natural rubber latex [12]. They also have a strong effect on the stability of high ammonia (HA) concentrated latex due to the adsorption of metal ions on the surface of rubber particles [12]. In addition, the metal ions have a direct effect on molecular weight, branching and gel content, especially on the storage characteristics of natural rubber [13]. The introduction of a certain amount of metal ion into polymers that contain ionic groups may also exert an important role on their mechanical properties [13]. It has been recognized that the elements that are commonly found in NR latex are Ca, K, Al, Na, Mg, Mn, Fe, Si, Rb, P, N, S and O. It was found that the mono-, di- and multivalent metal ions affected on the viscosity of NR latex [14]. Epoxy resin cured with metal-aromatic diamine complexes of copper (II) chloride and ortho-phenylene diamine (OPD) was also studied. It was found that the differences in the viscosity profiles for formulations with different metal contents indicates the network formation from the reaction of the epoxy and metal complex [15]. Recently, the self-healable ENR has been prepared by reacting with mixed metals ions and diamine crosslinking agents. It was found that some physical properties of the metal ion crosslinked samples are comparable with the conventional sulfur crosslinked samples [16]. In our previous work, the crosslinking reaction of epoxidized natural rubber (50 mol% epoxy, ENR-50) by metal ion namely ferric ion (Fe^{3+} , $FeCl_3$, ferric chloride) was investigated

and found that a small amount of $FeCl_3$ can cure ENR to a considerable extent. This might be attributed to chemical reaction between opened oxirane ring products of the ENR molecules and reactive Fe^{3+} ion to form crosslinking network structures via $-O-Fe-O-$ linkages [17]. Furthermore, the reaction of ferric chloride with ethylene oxide or propylene oxide was described and the structures of the reaction products indicate that ‘internal polymerization’ take place [18]. Therefore, the epoxy group containing molecules like ENR can even undergo a ‘internal polymerization’ type of reaction and yield many exchanged and complicated polymeric microstructures with very strong and dense crosslinking structures, as described in our previous work [17].

Nanocomposites based on elastomer and carbon nanotubes (CNTs) have been found in various applications with high thermal stability and electrical conductivity [19–21]. However, the decent properties of ENR/CNT nanocomposites depend mainly on dispersion and distribution of CNTs and their three-dimensional network formation in ENR matrix. Typically, CNTs have high aspect ratio and strong van der Waals forces among the particles that cause strong agglomeration of CNTs in ENR matrix [22]. Thus, addition of carbon nanotubes based filler in ENR has been widely studied with the main aims to enhance various ENR properties including cure characteristics, mechanical properties, thermal stability and electrical conductivity [23–27]. Also, CNTs have been used as a hybrid filler in combination with other types of fillers in different rubber composites, for instance in chloroprene rubber (CR) [28] and in solution styrene butadiene rubber (S-SBR) filled with the hybrid filler consisting of the multi-walled carbon nanotubes and ionic liquid (IL) [29]. It was found that the NR/CNT with IL hybrid nanocomposite indicates comparatively high electrical conductivity with lower percolation threshold concentration than in the NR/CNT without IL [30].

In the present work, epoxidized natural rubber (ENR) was compounded with ferric chloride to assist the crosslinking reaction and then filled with carbon nanotubes via the melt mixing method. Various properties, including cure characteristics, crosslink densities, mechanical, dynamic, morphological, and electrical properties, together with thermal resistance, were investigated with this ferric ion crosslinked and CNTs filled ENR composites.

2. Experimental

2.1. Materials

Epoxidized natural rubber with epoxide content of 50 mol% (ENR-50) was manufactured by Muang Mai Guthrie Co., Ltd., (Surat Thani, Thailand). The multi-wall carbon nanotubes (CNTs, NC7000) with 9.5 nm diameter, 1.5 μm length, and 90% purity, were manufactured by Nanocyl S.A. (Sambreville, Belgium). Ferric chloride (FeCl_3) was manufactured by Sigma-Aldrich Pte. Ltd. (Darmstadt, Germany).

2.2. Preparation of ENR- FeCl_3 /CNT nanocomposites

The ENR-50 was first compounded with an optimum dose of FeCl_3 at 7 mmol, according to our previous work [17]. The mixing was performed by a tangential internal mixer (Brabender Plasticorder with Mixer 50 EHT model: 835205 (Duisburg, Germany) at 60 °C with a rotor speed of 60 rpm and a total mixing time of 8 min (Table 1). The ENR-50 was first masticated for about 2 mins and then 7 mmol of FeCl_3 was added and continued mixing to reach the total mixing time of 8 min. In the preparation of ENR-50/CNTs nanocomposites, various loadings of CNTs (1, 3, 5, 7 and 10) were each mixed in the ENR-50/ FeCl_3 compound and continued mixing to reach the total mixing time of 8 min. The CNTs in powder form were gradually incorporated into the mixing chamber until they almost became a homogeneous mix with the ENR before closing the mixing chamber. The incorporated time of CNTs was set at about 4 min before further mixing was performed until the end of the mixing cycle at 8 min. The ENR- FeCl_3 /CNT compound was then dumped from the mixing chamber and passed through the 1 mm nip of an open two-roll mill, model YFCR 600, Yong Fong Machinery Co., Ltd. (Samut Sakorn, Thailand) at an ambient temperature for many cycles, involving cutting and banding of the rubber compounds. This was aimed to have better dispersion and distribution of the CNTs in the ENR matrix. The rubber compound was conditioned in a desiccator at room temperature for about 24 hrs. Cure characteristic was investigated

by a moving die rheometer (MDR), model: 81001 MDR 2000, Alpha Technologies, (Ohio, USA) at 160 °C. Finally, the compression molding PR1D-W400L450PM compression molding machine, Chareon Tut Co., Ltd, (Bangkok, Thailand) was used to prepare the ENR-50 vulcanizate sheet at 160 °C using the respective cure time based on the rheometer test.

2.3. Cure characterization

Cure characteristics of rubber compounds were determined at 160 °C by a moving die rheometer (MDR 2000), Alpha Technologies, (Ohio, USA) with a fixed frequency of 1.67 Hz and strain amplitude of 1° arc. The optimum scorch time (t_{s1}), cure time (t_{c90}), minimum torque (M_L), maximum torque (M_H), and torque difference ($M_H - M_L$), were determined from the curing curves.

2.4. Attenuated total reflection Fourier transform infrared (ATR-FTIR) spectroscopy

Attenuated total reflection Fourier transform infrared (FTIR) spectroscopy was performed using a Perkin-Elmer Spectrometer, Spectrum Two, Vertex70, Bruker (Karlsruhe, Germany). Different samples, including ENR- FeCl_3 compound and ENR- FeCl_3 /CNT nanocomposites were characterized by ATR-FTIR. The analysis was performed over the wide wavenumber ranges from 4000 to 400 cm^{-1} .

2.5. Mechanical properties

The tensile test specimens were mechanically prepared by cutting from the vulcanized rubber sheet to form a dumb bell shape specimen according to ISO 527 (type 5A). The samples were then clamped with the sample holder of the tensile testing machine, Zwick GmbH & Co., KG (Ulm, Germany). The test was then performed at room temperature by extending the samples with a crosshead speed of 200 mm/min according to ISO 527. The hardness was also determined by durometer Shore A, Instron (Norwood, USA), according to ISO 868.

2.6. Payne effect

The Payne effect was determined by measuring the storage modulus as a function of strain amplitude by using a rubber process analyzer, RPA 2000, Alpha Technologies (Ohio USA). The test was performed by measuring the storage shear modulus (G') of each filled un-vulcanized rubber compound under shear

Table 1. Compounding formulations of ENR-50 compounds.

Ingredient	Quantity [phr]	Mixing time [min]
ENR-50	100	2
CNTs	0, 1, 3, 5, 7 and 10	4
FeCl_3	7 mmol	2

deformation with strain amplitude ranges from 0.56 to 100% at the fixed frequency of 1.0 Hz and 100 °C. The Payne effect was quantified by the difference of storage moduli at very low strain ($G'_{0.56}$) and at very high strain (G'_{100}). That is, the Payne effect is typically estimated from the difference between moduli at very low and very high strain regimes (*i.e.*, $G'_0 \rightarrow G'_{100}$) [31], as Equation (1):

$$G'_0 - G'_{100} = \Delta G' \quad (1)$$

where G'_0 and G'_{100} are the minimum (*i.e.*, $G'_{0.56}$) and the maximum storage moduli (*i.e.*, at the strain amplitude 100%).

2.7. Electrical properties

Electrical properties of the ENR-FeCl₃ compound and ENR-FeCl₃/CNT nanocomposites in terms of electrical conductivity (σ) and dielectric constant (ϵ') were measured at room temperature by an LCR meter, Hioki IM 3533, Hioki E.E. Corporation (Nagano, Japan) in the frequency ranges of 1 to 10⁵ Hz. The LCR meter was connected to the electrode plates of a dielectric test fixture model 16451B dielectric test fixture, Test Equipment Solutions Ltd. (Berkshire, United Kingdom), with a 5 mm electrode diameter. The electrical conductivity (σ), and dielectric constant (ϵ') were determined as Equations (2) and (3) [32, 33]:

$$\sigma = \frac{1}{\rho} = \frac{d}{(R_p)A} \quad (2)$$

$$\epsilon' = \frac{C_p(d)}{A(\epsilon_0)} \quad (3)$$

where d and A refer to the sample thickness and the area of an electrode, respectively. The parameter ϵ_0 is the dielectric constant of the free space, which is $8.854 \cdot 10^{-12}$ F/m. The factor ρ is the volume resistivity which is reciprocal of conductivity.

2.8. Bound rubber contents

Bound rubber contents of the ENR-FeCl₃/CNTs nanocomposites were estimated by the swelling method [34]. The sample was initially immersed in toluene and conditioned to the equilibrium state for at least 72 h, renewing the toluene every 24 h. The sample was later separated from the solvent and then dried at 105 °C for at least 24 h. In the same manner, the ENR compound sample was immersed in toluene

for at least 72 h at room temperature, either in the normal state or in an ammonia atmosphere, with the renewal of toluene every 24 h. Then, the solvent was separated, dried at 105 °C for 24 h and eventually weighted. It is noted that ammonia was used to cleave the physical linkages between rubber molecules and filler surfaces. The bound rubber content was then determined as Equation (4) [34]:

$$\text{Bound rubber content [\%]} = \frac{W_{fg} - W_f}{W_p} \cdot 100 \quad (4)$$

where W_f and W_p are the weights of filler and rubber in the specimens, respectively. W_{fg} is the weight of filler with bound rubber absorbed on it after toluene extraction [34].

2.9. Thermogravimetric analysis (TGA)

Thermal stability of the ENR-FeCl₃ compound and ENR-FeCl₃/CNT nanocomposites was examined by thermogravimetric analysis using TGA-SDTA 851, Mettler Toledo (Zurich, Switzerland). The measurement was performed under a nitrogen atmosphere at 30–600 °C before switching to an oxygen atmosphere until 900 °C with the same heating rate of 10 °C /min.

2.10. Dynamic mechanical analysis

Dynamic mechanical analysis (DMA) was carried out using Perkin Elmer DMA 8000 Perkin Elmer Inc. (Waltham, USA) in a tension mode in the temperature ranges from –100 to 80 °C with a heating rate of 3 °C/min and a fixed deformation frequency of 1 Hz.

2.11. Morphological characterization

The morphological properties of the ENR-FeCl₃ compound and ENR-FeCl₃/CNT nanocomposites were characterized by scanning electron microscopy (SEM), Quanta 250, FEI Company (Černovice, Czech Republic). Each specimen was first cryogenically cracked in liquid nitrogen to create a fresh cross-sectional surface. Then, the dried surface was gold coated and examined by SEM.

3. Results and discussion

3.1. Cure characteristics

Figure 1 shows torque-time curves or cure curves of the ENR-FeCl₃ compounds in combination with different CNTs loadings at 1, 3, 5, 7 and 10 phr (*i.e.*, F7C1, F7C3, F7C5, F7C7 and F7C10, respectively).

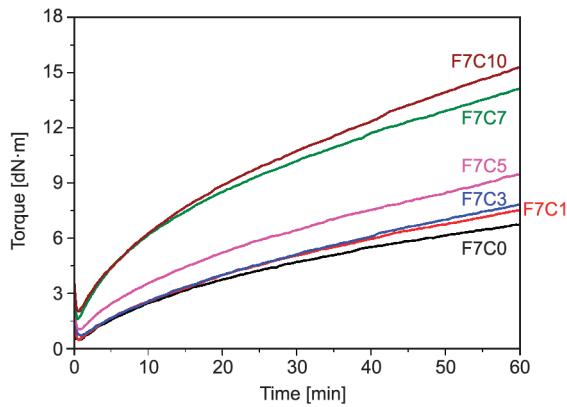


Figure 1. Mixing torque-time curves of ENR-FeCl₃ compound without (F7C0) and with various CNTs loadings at 1, 3, 5, 7 and 10 phr (*i.e.*, F7C1, F7C3, F7C5, F7C7 and F7C10).

It is seen that the cure curves of all ENR-FeCl₃ compounds exhibited the marching cure behavior, *i.e.*, an increase in mixing torques as increasing of mixing time. This is due to internal polymerization of the epoxy group resulting crosslinking network. Most probably the reaction is not complete as there are many epoxy groups which are available for

the further reaction. The reaction mechanism is further illustrated between Fe³⁺ in FeCl₃ molecules and epoxy group of ENR to form –O–Fe–O– linkages, as shown in a proposed reaction in Figures 2 and 3. The participation of the internal polymerization of oxirane rings of ENR molecules is also described as the chemical reaction shown in Figure 4. It is noted that under the given conditions at high temperature and shear force, the oxirane rings in ENR molecules are prone to ring opening reaction with a product that are capable of forming new linkages with another ring opened ENR fragment via Fe³⁺ bridge, as described in our previous work [17]. Furthermore, the epoxy group containing molecules can even undergo a ‘internal polymerization’ type of reaction and yield many exchanged and complicated polymeric microstructures which can result in very strong crosslinking structures, as described in our previous work [17]. Therefore, increasing trend of curing rheometric torque (Figure 1) and hence crosslink density based on torque difference (Table 2) are seen. In Figure 1, it is also seen that the cure curves of ENR-FeCl₃/CNTs nanocomposite show higher marching cured

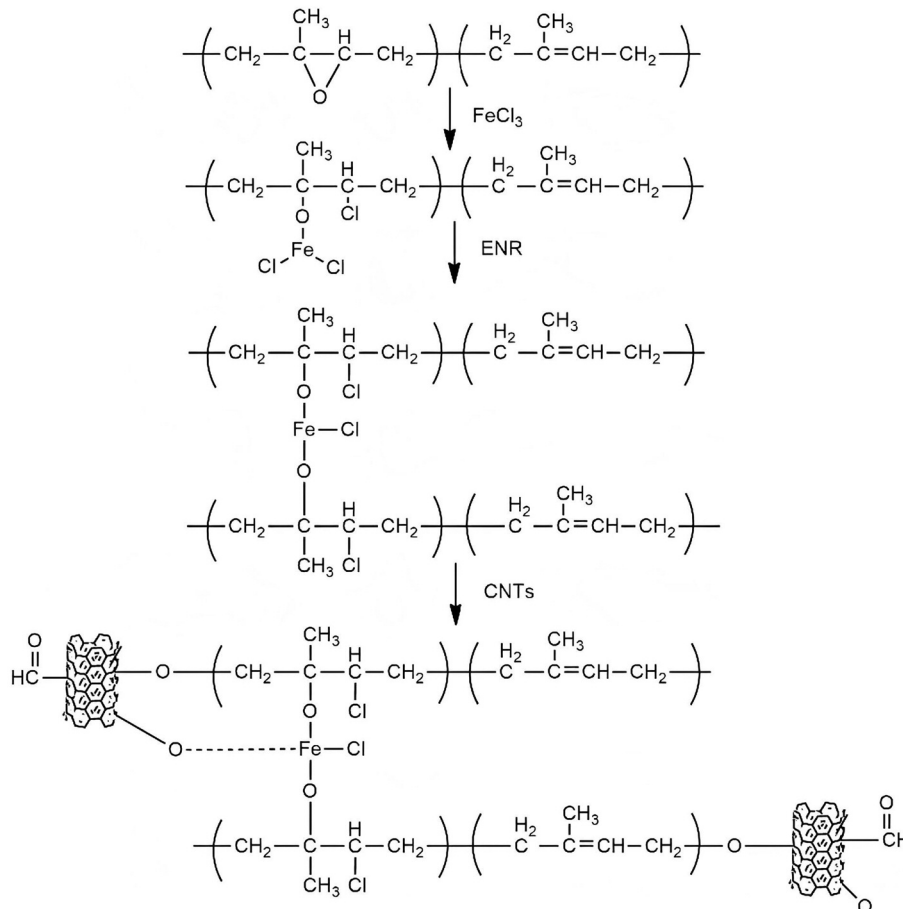


Figure 2. A proposed reaction mechanism among epoxidized natural rubber, ferric chloride and carbon nanotubes. The nucleophilic chloride is attached with α position with respect to the methyl group.

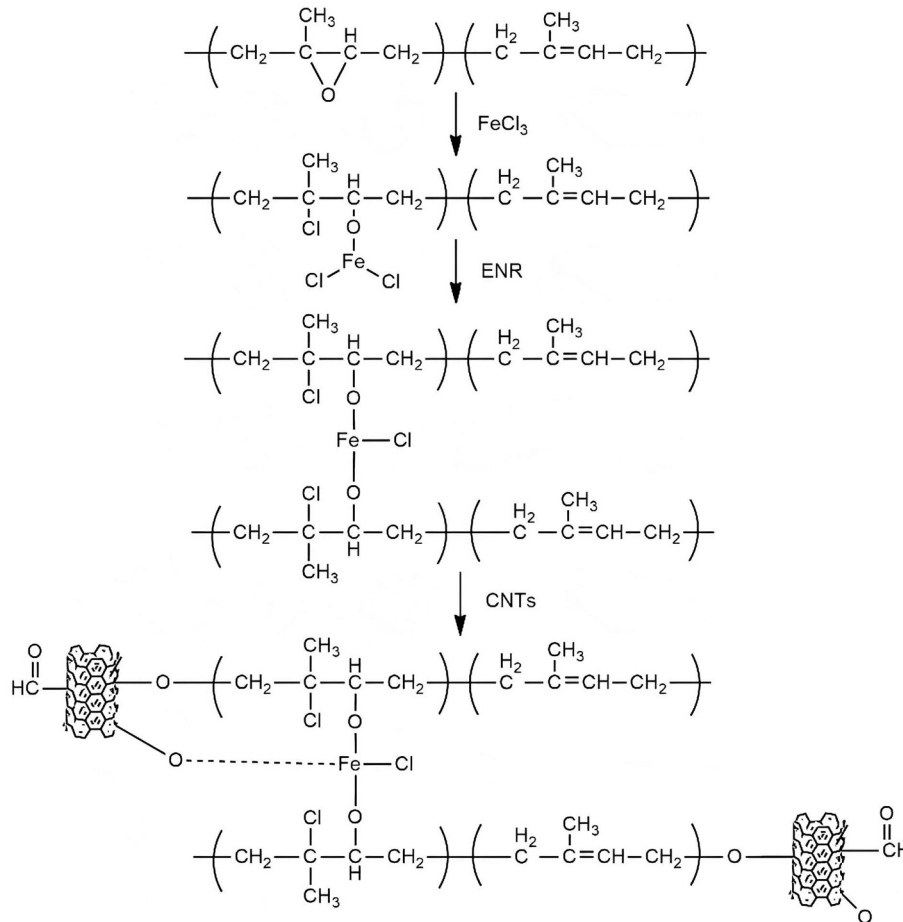


Figure 3. A proposed reaction mechanism among epoxidized natural rubber, ferric chloride and carbon nanotubes. The nucleophilic chloride is attached with β position with respect to the methyl group.

curves, indicating by a dramatically increase in torques with increasing testing time and increasing loadings of the CNTs. This reflects that the ENR-FeCl₃/CNTs compounds require longer time to complete the crosslinking reaction. Table 2 shows cure characteristics in terms of minimum torque (M_L), maximum torque (M_H), torque difference or delta torque ($M_H - M_L$), scorch time (T_{s2}) and cure time

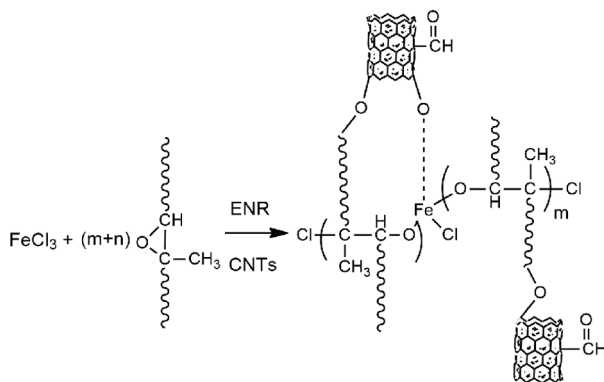


Figure 4. A proposed reaction mechanism of ‘internal polymerization’ of epoxy groups of epoxidized natural rubber with ferric chloride and carbon nanotubes.

(T_{c90}) of ENR-FeCl₃ without and with different loadings of CNTs. It can be seen that incorporation of CNTs causes acceleration of the curing reaction of ENR-FeCl₃ compounds by reducing of scorch time (T_{s2}) and cure time (T_{c90}) together with raising of the cure rate index (CRI). This might be due to higher thermal conductivity of FeCl₃ and CNTs that cause enhancing and accelerating of the curing reaction of the ENR and FeCl₃ together with internal polymerization of epoxide groups and hence increasing of the chemical interaction between polar functional groups in ENR and CNTs surface [22]. Also, incorporation of CNTs caused higher torque difference (Table 2) that reflects higher crosslinking structures and reinforcement of the ENR vulcanizates. Furthermore, increasing loading level of CNTs causes an increase in thermal conductivity of the ENR compound that may facilitate and hence accelerate the curing reaction. Also, higher possibility of the polar functional groups on the CNT surfaces can interact with the epoxide groups of ENR and their opened ring products.

Table 2. Cure characteristics in terms of minimum torque (M_L), maximum torque (M_H), torque difference ($M_H - M_L$), scorch time (T_{s2}) and cure time (T_{c90}) of ENR-FeCl₃ without and with CNTs.

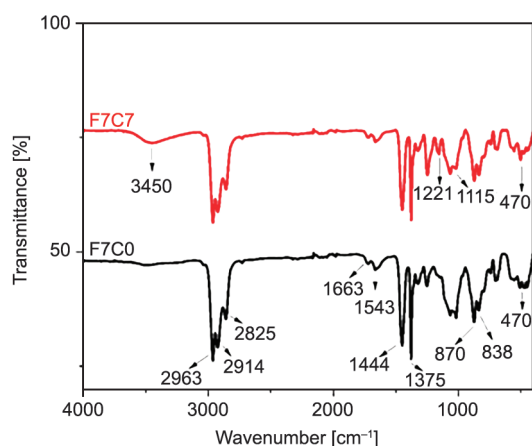
Compounds	M_L [dN·m]	M_H [dN·m]	$M_H - M_L$ [dN·m]	T_{s2} [min]	T_{c90} [min]	CRI
F7C0	0.48	6.75	6.27	2.20	7.40	19.23
F7C1	0.76	7.53	6.77	2.11	7.38	18.98
F7C3	0.83	7.84	7.01	2.02	6.72	21.27
F7C5	1.06	9.48	8.42	1.60	6.34	21.10
F7C7	1.62	14.15	12.53	1.32	5.91	21.78
F7C10	2.02	15.31	13.29	1.21	5.58	22.88

3.2. Attenuated total reflection (ATR) Fourier transform infrared spectrophotometer (FTIR)

Figure 5 shows ATR-FTIR spectra of ENR-FeCl₃ compounds without and with CNTs loading at 7 phr. Also, the peak assignments for the FTIR spectra in Figure 5 are listed in Table 3. It can be seen that the absorption peaks for the characteristic of ENR

Table 3. Peak assignments for ENR-FeCl₃ compound with 7 mmol FeCl₃ (F7C0) without and with 7 phr CNTs (*i.e.*, F7C7) for the FTIR spectra in Figure 3.

Wavenumber [cm ⁻¹]	Assignment
2963	-CH ₃ stretching vibration
2914	-CH ₂ stretching vibration
2825	-CH ₂ stretching vibration
1663	C=C stretching vibration
1543	N-H bending vibration of amide
1375	-CH ₃ bending vibration
1221	C-O stretching vibration of CNT
1115	C-O stretching vibration of CNT
870	C-O stretching vibration of ENR
835	=C-H out of plane bending
470	Fe-O stretching vibration

**Figure 5.** ATR-FTIR spectra of ENR-FeCl₃ compound with 7 mmol FeCl₃ (F7C0) without and with 7 phr CNTs (*i.e.*, F7C7).

molecules are seen at the wavenumbers of 1663 and 1543 cm⁻¹, which are assigned to C=C stretching and N-H bending vibrations of mono-substituted amide II in ENR molecules, respectively [35]. Also, the FTIR absorption peak characteristic of ENR molecules is seen at the wavenumber of 870 cm⁻¹, which indicates the C-O stretching vibration of ENR molecules (Table 3). Furthermore, the absorption peaks at the wavenumbers 2825 and 2914 cm⁻¹ that assign to -CH₂ stretching vibrations are clearly seen. In addition, the absorption peak at 2963 and 1375 cm⁻¹ which are assigned to -CH₃ stretching vibrations and -CH₃ bending vibrations in the ENR molecules are also seen, respectively. In both FTIR spectra, the absorption peak at the wavenumbers of 835 cm⁻¹ is observed. It corresponds to =C-H out of plane bending in ENR molecules. Furthermore, the absorption peak at 470 cm⁻¹ which reflects the Fe-O stretching vibration in the ENR-FeCl₃ and Fe-O stretching vibration in the functional group on the CNTs surface, are clearly seen [36]. In Figure 5, it is also clear that the ENR-FeCl₃/CNTs nanocomposite shows significant absorption peaks at similar locations as the FTIR peaks of the ENR-FeCl₃ compound without CNTs but with lower peak intensities. This may be attributed to the chemical interactions of polar functional groups in ENR molecules and polar groups on the CNT surfaces. Moreover, the addition of CNTs gives rise to a new absorption peak at wavenumbers 1221 cm⁻¹, which is assigned to C-O stretching vibrations of polar functional groups on the CNTs surfaces [37].

3.3. Mechanical properties

Figure 6 shows stress-strain curves of ENR-FeCl₃ compound without CNTs (*i.e.*, F7C0) and with various CNTs loadings at 1, 3, 5, 7 and 10 phr (*i.e.*, F7C1, F7C3, F7C5, F7C7 and F7C10, respectively). Also, mechanical properties in terms of 100% modulus,

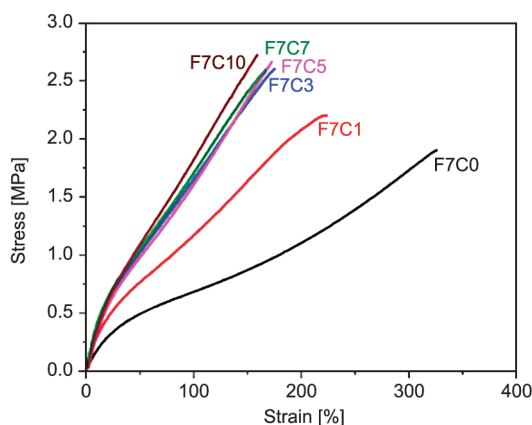


Figure 6. Stress-strain curves of ENR-FeCl₃ compound without (F7C0) and with various CNTs loadings at 1, 3, 5, 7 and 10 phr as denoted by F7C1, F7C3, F7C5, F7C7 and F7C10, respectively.

tensile strength, elongation at break and hardness (Shore A) of various ENR-FeCl₃ compounds without and with CNTs are summarized in Table 4. It is clearly seen that the addition and increasing CNTs loadings affect the characteristic of the stress-strain behavior of ENR vulcanizates by a significant increase in Young's moduli (*i.e.*, slope at the initial part of the curves), 100% moduli, and tensile strength as compared with the F7C0 compound without CNTs (Table 4). This is due to the formation of stronger three-dimensional networks based on the reaction of Fe³⁺ and oxirane rings and the internal polymerization of oxirane groups in ENR molecules. Furthermore, higher chemical interaction among the polar functional groups at the CNTs surfaces and oxirane rings in ENR molecules causes higher reinforcement as increasing of the CNTs loadings. In Figure 6 and Table 4, it is also seen that a decrease in elongation at break is seen upon increasing of CNTs loadings. However, similar levels of moduli, tensile strength and elongation at break are seen in the ENR-FeCl₃/CNTs nanocomposites with CNTs loadings at 7 and 10 phr. This may be due to the re-agglomeration of

CNTs owing to an excess amount of solid particulates inside the ENR matrix. In Table 4, it is also clear that the hardness of the ENR-FeCl₃/CNTs nanocomposites increases with an increase in CNTs loadings. This is attributed to an increase in the degree of crosslinks between ENR-50 molecules via –O–Fe–O– linkages, and internal polymerization of the epoxirane rings. Also, the chemical interaction among polar functional groups in ENR and CNTs, together with higher rigidity due to a higher amount of solid CNTs are other main reasons for an increase in hardness.

3.4. Payne effect

Figure 7 shows the storage modulus (G') as a function of strain amplitude of ENR-FeCl₃ with 7 mmol of FeCl₃ (F7C0) without and with various CNTs loadings at 1, 3, 5, 7 and 10 phr. It can be seen that the F7C0 compound without CNTs exhibits the lowest storage modulus at a given strain amplitude. However, the storage modulus is increased after the incorporation of CNTs and increasing CNTs loadings. The storage moduli of all samples showed a decreasing trend as increasing strain amplitude over 10% magnitude. This may be due to the shearing forces causing breaking down of the CNTs networks or agglomerates under high temperature conditions [38]. The Payne effect has been typically used to verify the filler-filler and filler-rubber interactions in a rubber composite [39]. It can be assessed from a decreasing trend of the storage modulus (G') as increasing the strain amplitudes. In Figure 7, a slight decreasing trend of storage modulus is also seen in the F7C0 compound without CNTs. It may arise from the chain disentanglement of ENR molecules together with a breakdown of crosslinked networks under high shear stress and high heat [40]. On the other hand, the ENR-FeCl₃/CNTs nanocomposites show the typical Payne effect, which indicates the breakdown of filler-filler interactions. It is clear in Figure 7

Table 4. Mechanical properties in terms of 100% modulus, tensile strength, elongation at break and hardness (Shore A) of ENR-FeCl₃ compounds without (F7C0) and with CNTs at 1, 3, 5, 7 and 10 phr (*i.e.*, F7C1, F7C3, F7C5, F7C7 and F7C10, respectively).

Materials	100% modulus [MPa]	Tensile strength [MPa]	Elongation at break [%]	Hardness [Shore A]
F7C0	0.89±0.18	1.89±0.11	325.7±20.2	44.5±1.0
F7C1	1.17±0.22	2.20±0.35	223.1±18.5	45.6±1.1
F7C3	1.65±0.15	2.60±0.23	174.9±22.2	58.3±3.1
F7C5	1.71±0.10	2.71±0.17	174.5±15.6	61.1±1.5
F7C7	1.72±0.13	2.76±0.24	166.2±17.7	73.7±1.3
F7C10	1.75±0.18	2.81±0.43	166.3±13.3	76.6±2.0

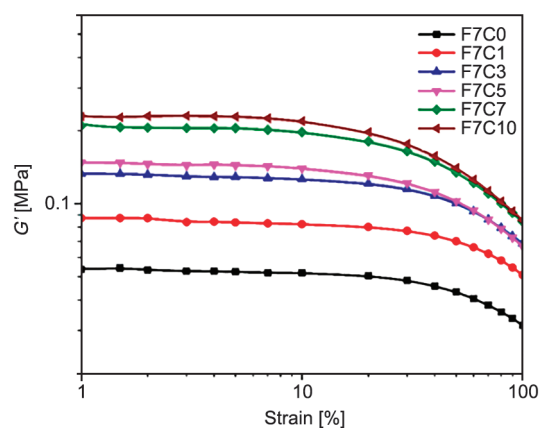


Figure 7. Storage modulus as a function of strain amplitude of ENR-FeCl₃ compound with 7 mmol of FeCl₃ (F7C0) without and with different CNTs loadings.

Table 5. Storage modulus at very low strain ($G'_{0.56}$) and at very high strain (G'_{100}), and their difference ($\Delta G'$) of ENR-FeCl₃ compound without and with CNTs.

Compounds	$G'_{0.56}$ [MPa]	G'_{100} [MPa]	$\Delta G'$ [MPa]
F7C0	0.04	0.03	0.01
F7C1	0.09	0.05	0.04
F7C3	0.13	0.07	0.06
F7C5	0.17	0.07	0.10
F7C7	0.20	0.08	0.12
F7C10	0.25	0.09	0.16

that the Payne effect is more prominent in the nanocomposites with higher CNTs loadings. Table 5 shows storage moduli at very low strain ($G'_{0.56}$) and at very high strain amplitudes (G'_{100}), as well as the storage modulus difference ($\Delta G'$) of the ENR-FeCl₃ compound with 7 mmol of FeCl₃ (F7C0) without and with various CNT loadings at 1, 3, 5, 7 and 10 phr. It can be seen that a strong decrease in storage modulus with an increase in the Payne effect in terms of the difference in storage modulus ($\Delta G'$) is clearly seen with increasing in the CNTs loadings. This implies that strong CNTs agglomeration is present in the ENR matrix with higher CNTs loadings [41]. Moreover, the lowest Payne effect was observed in the F7C0 without CNTs ($\Delta G' = 0.01$). This is due to solely the breakdown of molecular chain entanglement of ENR molecules and of the linkages in ENR crosslinking networks, and also a breakdown of small FeCl₃ clusters that remain in the ENR matrix. Therefore, it is concluded that the higher Payne effect in ENR-FeCl₃/CNTs nanocomposites relates to the breakdown of strong filler-filler interactions [42].

3.5. Morphological properties

Figure 8 shows SEM micrographs of ENR-FeCl₃ compound without and with different CNTs loadings at 1, 3, 5, 7, and 10 phr. It can be seen that F7C0 without CNTs shows homogeneous dispersion of solid particles of FeCl₃ in the ENR matrix (Figure 8a). However, in the ENR-FeCl₃/CNTs nanocomposites with CNTs loadings at 1, 3, 5 and 7 phr, large agglomerates are absent rather, some small CNTs aggregates are clearly seen in Figure 8b to Figure 8e. This indicates good dispersion of CNTs in ENR-FeCl₃ and may be good compatibility between CNTs and the ENR-FeCl₃ compounds. On the other hand, in Figure 8f, large agglomerates are clearly seen in the ENR-FeCl₃ compound with 10 phr of CNTs. This is due to re-agglomeration of excess amount of CNTs in the ENR matrix, causing poorer dispersion, distribution and hence stronger CNTs agglomeration in ENR matrix.

3.6. Bound rubber contents

Table 6 shows the bound rubber/gel content contents of ENR-FeCl₃ compound without and with various CNTs contents. It is found that the F7C0 sample without CNTs shows a slight gel-like content in the bound rubber experiment. In the present case, most probably, FeCl₃ started to react with epoxy group even at room temperature or during the shear mixing condition, resulting in a gel-like formation in the experiment. The presence of FeCl₃ is also cannot be ruled out. It is clearly seen that the bound rubber content increases with an increase in CNTs loadings. This is due to an increase in filler-rubber interactions between ENR and polar functional groups at the CNTs surface. It is also seen that the ENR-FeCl₃ compound with CNTs showed much larger bound rubber contents than that of the ENR-FeCl₃ compound without CNTs, especially in the ENR nanocomposite with CNTs loadings higher than 5 phr. Also, the ENR-FeCl₃/CNTs nanocomposite with 7 phr of CNTs reaches the optimum bound rubber content due to the finer dispersion and distribution of CNTs in the ENR matrix (Figure 8). Increasing CNTs loading to 10 phr causes a small increase in bound rubber content due to the large agglomeration of CNTs, as shown in Figure 8e.

3.7. Thermogravimetric analysis (TGA)

Figure 9 shows the TGA and DTG thermograms of the ENR-FeCl₃ compound without and with various

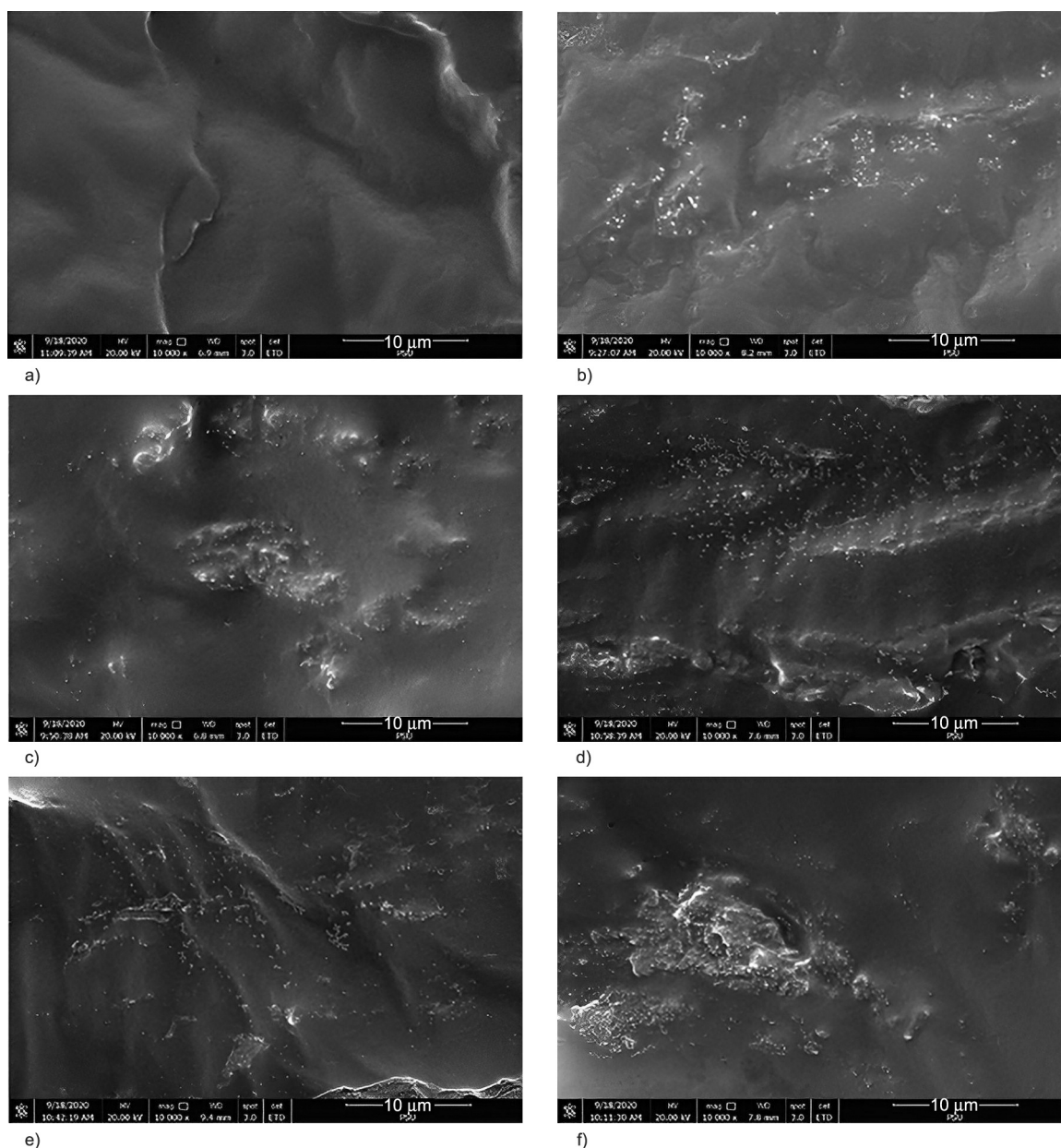


Figure 8. SEM micrographs of ENR-FeCl₃ compound with 7 mmol of FeCl₃ (F7C0) without (a) and with various CNTs loadings at 1 phr (b), 3 phr (c), 5 phr (d), 7 phr (e), and 10 phr (f).

Table 6. Bound rubber contents of ENR-FeCl₃ compound with FeCl₃ without and with various CNTs loadings determined by equilibrium swelling measurements.

Sample	Bound rubber contents [%]
F7C0	1.09
F7C1	18.79
F7C3	22.37
F7C5	36.17
F7C7	42.31
F7C10	42.56

concentrations of CNTs at 1, 3, 5, 7 and 10 phr. It is noted that TGA was performed under a nitrogen atmosphere in the temperature range 30–600 °C, before

switching to an oxygen atmosphere and heated until 900 °C with the same heating rate at 10 °C/min. In **Figure 9a**, the first degradation step under N₂ atmosphere of various ENR compounds is seen in the temperature range of 255–265 °C. This is clearly indicated by the first DTG peaks in **Figure 9b** and T_{d1} in **Table 7**, which associates to the dissociation of chlorine atoms in FeCl₃ molecules. In addition, the second DTG peaks are seen at around 420–430 °C (*i.e.*, T_{d2} in **Table 7**), due to the decomposition of the hydrocarbon in ENR molecules. It is clear that the second degradation peak height decreases with the increase of the CNTs loading. This is activated by higher thermal conductivity due to FeCl₃ and CNTs

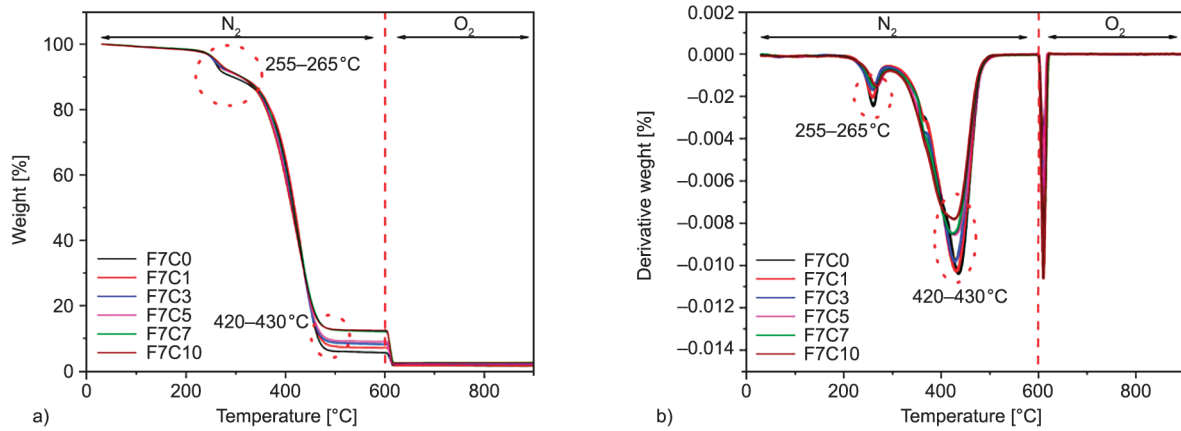


Figure 9. TGA (a) and DTG thermograms (b) of ENR-FeCl₃ compound with 7 mmol of FeCl₃ (F7C0) without and with different loadings of CNTs at 1, 3, 5, 7 and 10 phr.

Table 7. Degradation temperature (T_d) and weight losses of ENR-50 compound with 7 mmol of FeCl₃ (F7C0) without and with various CNTs loadings at 1, 3, 5, 7 and 10 phr.

Sample	T_{d1} [°C]	T_{d2} [°C]	Weight loss under the nitrogen atmosphere		Weight loss under the oxygen atmosphere	
				[%]		[%]
F7C0	258.7	430.3		90.14		1.15
F7C1	259.9	429.0		91.24		1.99
F7C3	260.1	427.8		91.37		2.03
F7C5	260.8	425.6		91.89		2.34
F7C7	261.2	424.2		91.93		2.62
F7C10	261.4	420.1		92.48		2.67

particles which are thoroughly dispersed in the ENR matrix. Nevertheless, in Figure 9a and Table 7, in the last region of TGA thermograms under oxygen atmosphere, it is clearly seen that the ENR-FeCl₃/CNTs nanocomposites have higher remained residues than the ENR-FeCl₃ without CNTs. Also, the residue contents decrease with an increase in the CNTs loadings. This is due to higher chemical interaction among the polar functional groups on CNTs surfaces and polar functional groups in ENR molecules together with more char residue contents in CNTs.

3.8. Dynamic mechanical analysis (DMA)

Figure 10 shows storage modulus (G') and loss tangent ($\tan \delta$) as a function of temperature for ENR-FeCl₃ compound without (F7C0) and with various CNTs loadings at 1, 3, 5, 7 and 10 phr. It can be seen that the storage moduli in the glassy region of ENR-FeCl₃/CNTs composites are higher than the F7C0 without CNTs. Also, the storage moduli increase with an increase in CNTs loadings. This may be due to higher reinforcement of ENR by CNTs particles, resulting in stronger CNTs and rubbery networks.

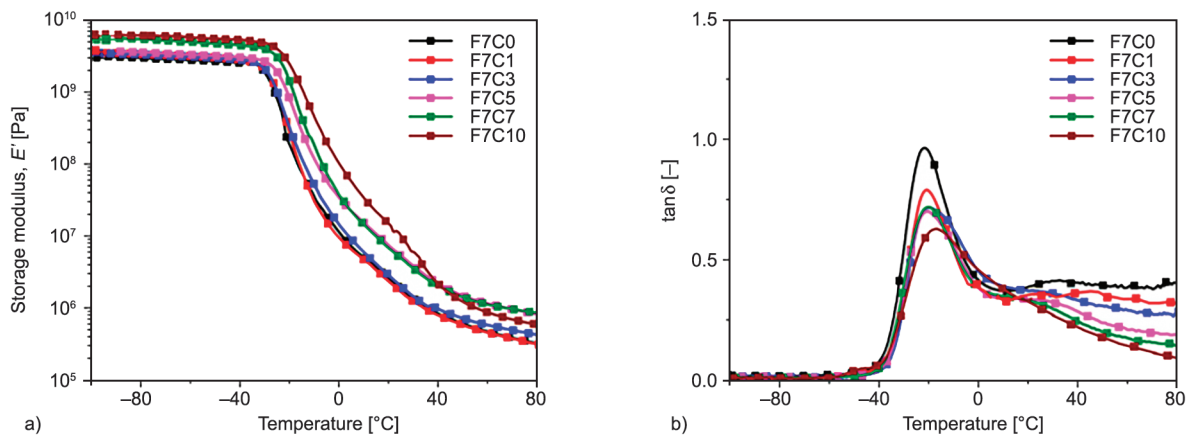


Figure 10. Storage modulus (a) and $\tan \delta$ (b) as a function of the temperature of ENR-FeCl₃ compound with 7 mmol of FeCl₃ (F7C0) without and with various CNTs loadings at 1, 3, 5, 7 and 10 phr.

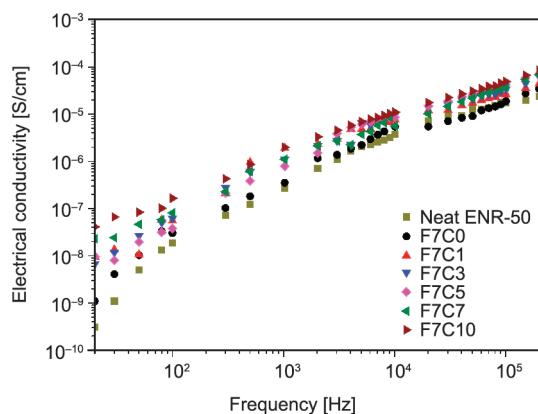
Table 8. Glass transition temperature (T_g) of ENR-50 compound with 7 mmol of FeCl_3 (F7C0) without and with various CNTs loadings at 1, 3, 5, 7 and 10 phr.

Samples	Glass transition temperature [°C]
F7C0	-20.3
F7C1	-20.1
F7C3	-19.7
F7C5	-19.0
F7C7	-18.3
F7C10	-17.1

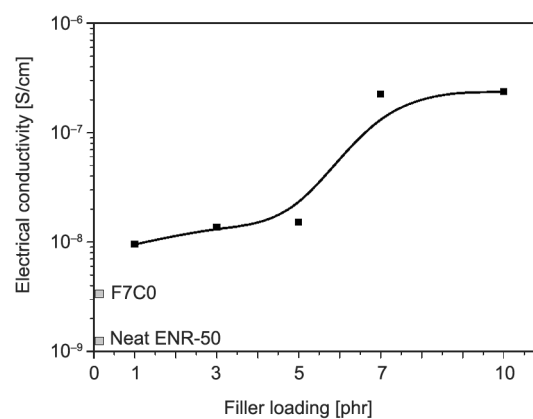
Also, more solid CNTs contents in the ENR nanocomposites cause the formation of higher stiffness materials. In Figure 10, it is also seen that the addition of CNTs in ENR causes shifting of the $\tan\delta$ peaks (Figure 10b) and glass transition temperature (T_g) (Table 8) toward higher temperature ranges as compared with the F7C0 without CNTs. This is attributed to more rigid ENR molecular networks with an increase in CNTs loadings due to interaction among polar functional groups at CNTs surfaces and the polar groups in ENR molecules. Even more free volume is obvious in the ENR matrix due to CNTs agglomeration with high CNTs loadings that may cause molecular rubber chains to move more freely [43]. However, the influence of chemical interaction on the thermal properties of the ENR- FeCl_3 /CNTs may play a more significant role. It results in an increase in T_g of ENR- FeCl_3 /CNTs nanocomposites with increasing of CNTs loadings.

3.9. Electrical properties

Figure 11 shows electrical conductivity as a function of the frequency of ENR- FeCl_3 compound with

**Figure 11.** Electrical conductivity as a function of frequency of ENR- FeCl_3 compound with 7 mmol of FeCl_3 (F7C0) without and with various CNTs loadings at 1, 3, 5, 7 and 10 phr.

7 mmol of FeCl_3 (F7C0) without and with various CNTs loadings at 1, 3, 5, 7 and 10 phr. It is seen that the electrical conductivity-frequency curves of the ENR- FeCl_3 /CNTs nanocomposites are located above the curve of the neat ENR-50 and F7C0 without CNTs. Also, it is clearly seen that the incorporation of CNTs in ENR causes a sudden improvement of the electrical conductivity of the ENR- FeCl_3 compound. In addition, the electrical conductivity increases with increasing concentrations of CNTs. Figure 12 shows the electrical conductivity at a frequency of 50 Hz at various CNTs loadings as compared with the neat ENR-50 and F7C0 compound without CNTs. It is clearly seen that the neat ENR-50 shows very low electrical conductivity (about $1.09 \cdot 10^{-9}$ S/cm). However, an abrupt increase in electrical conductivity to about $8.75 \cdot 10^{-6}$ S/cm is seen upon the addition of FeCl_3 in ENR to form F7C0. This is due to the higher electrical conductivity of Fe^{3+} that is present in the ENR matrix. Furthermore, electrical conductivity is gradually increased again with the incorporation of 1 phr of CNTs in the ENR matrix. This may be due to the higher electrical conductivity of CNTs networks in the ENR matrix. In Figure 12, it is also seen that an increase in CNTs loadings from 1 to 5 phr, cause a marginal increase in the electrical conductivity. However, a sudden increase in electrical conductivity is seen after adding of CNTs beyond 5 phr due to the formation of conductive CNTs networks. Therefore, the CNTs networks act as the bridge to carry electron charges throughout the ENR matrix, causing powerful transfers of electrons and significantly enhancing the electrical conductivity of the composites. It is noted that the CNTs concentration

**Figure 12.** Electrical conductivity at a frequency at 50 Hz of neat ENR-50, ENR- FeCl_3 compound with 7 mmol of FeCl_3 (F7C0) with various CNTs loadings at 1, 3, 5, 7 and 10 phr.

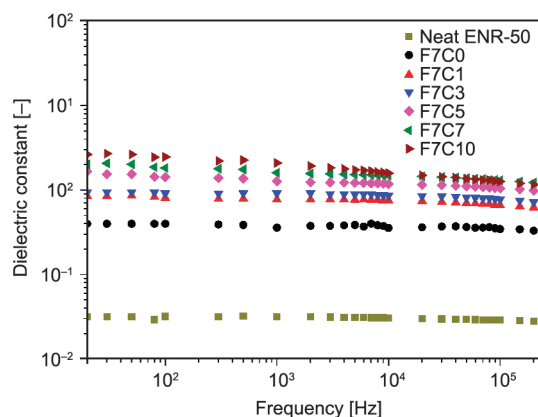


Figure 13. Dielectric constant as a function of the frequency of neat ENR-50, ENR-FeCl₃ compound with 7 mmol of FeCl₃ (F7C0) without and with various CNTs loading at 1, 3, 5, 7 and 10 phr.

that causes the formation of the fully CNTs network is called the percolation threshold concentration (PTC), which is about 7 phr of CNTs in this case (Figure 12). In such a case, three-dimensional CNTs networks are successfully formed in the ENR matrix. This may be attributed to strong filler-rubber interactions between oxirane rings in ENR molecules and polar functional groups on CNT surfaces.

Figure 13 shows the dielectric constant as a function of the frequency of the neat ENR-50 and ENR-FeCl₃ with 7 mmol of FeCl₃ (F7C0) without and with various CNTs. It is seen that the neat ENR-50 shows an independent dielectric constant with frequency. This may be due to poor polarization of the ENR molecular chains [9]. Moreover, the ENR-FeCl₃ has a higher dielectric constant than the neat ENR-50. It corresponds to the trend of electrical conductivity (Figure 11). In addition, the dielectric constant of the ENR-FeCl₃/CNTs compounds show a significantly increasing trend as the CNTs loading increases. It may be attributed to the sp²-hybridization in CNTs with abundant numbers of free electrons forming electric dipoles [6].

4. Conclusions

ENR-50 was successfully crosslinked by Fe³⁺ ion of FeCl₃ to form the coordination crosslinks (–O–Fe–O– linkages) between ENR molecules and to form internal polymerized oxirane groups of ENR molecules. In addition, the incorporation of CNTs improves various properties of ENR-FeCl₃ compounds, including tensile strength, dynamic properties, electrical

conductivity, and thermal properties. It is clearly seen that the ENR-FeCl₃ compounds filled with various CNTs loadings have higher torque differences and mechanical properties than the ones without CNTs. This is due to higher contents of the crosslinking structures of ENR, the three-dimensional CNTs networks, and the reinforcement effect of CNTs in the ENR matrix. SEM micrographs reveal very small CNTs aggregates in the ENR-FeCl₃ compounds with 5 and 7 phr of CNTs loadings, which indicate good dispersions of CNTs in the ENR matrix. However, ENR-FeCl₃ compound with 10 phr of CNTs shows a large agglomerate due to re-agglomerates of CNTs. According to DMA, glass transition temperature (T_g) increases with an increase in CNTs loadings due to more restrictions on chain mobility of ENR molecules. Furthermore, the ENR-FeCl₃/CNTs nanocomposites show improvement of storage modulus, 100% moduli, electrical conductivity, and dielectric constant as compared with the ENR-FeCl₃ compound without CNTs. It was also found that the ENR-FeCl₃/CNTs nanocomposites have the percolation threshold concentration at 7 phr of CNTs. It indicates the presence of the three-dimensional network, which is in agreement with the morphological properties. Also, the thermal resistance of ENR-FeCl₃/CNTs nanocomposites increases with an increase in CNTs loadings. This is due to the higher content of the coordination linkages of ENR-FeCl₃ and reinforced by CNTs.

Acknowledgements

This work was supported by Thailand Research Fund and National Research Council of Thailand for providing a Royal Golden Jubilee Ph.D. Program (Grant No. PhD/0121/2560). Also, some part of the scholarship was also supported by the Graduates School, Prince of Songkla University, Surat Thani Campus, Thailand. The Leibniz-Institut für Polymerforschung Dresden e. V. (IPF), Dresden, German, is also gratefully acknowledged for hosting Kriengsak Damampai during his research stay from October 2019 to March 2020 and providing additional experimental facilities and equipment.

References

- [1] Salaeh S., Nakason C.: Influence of modified natural rubber and structure of carbon black on properties of natural rubber compounds. *Polymer Composites*, **33**, 489–500 (2012).
<https://doi.org/10.1002/pc.22169>

- [2] Matchawet S., Kaesaman A., Bomlai P., Nakason C.: Electrical, dielectric, and dynamic mechanical properties of conductive carbon black/epoxidized natural rubber composites. *Journal of Composite Materials*, **50**, 2191–2202 (2016).
<https://doi.org/10.1177/0021998315602941>
- [3] Teh P. L., Mohd Ishak Z. A., Hashim A. S., Karger-Kocsis J., Ishiaku U. S.: Effects of epoxidized natural rubber as a compatibilizer in melt compounded natural rubber–organoclay nanocomposites. *European Polymer Journal*, **40**, 2513–2521 (2004).
<https://doi.org/10.1016/j.eurpolymj.2004.06.025>
- [4] Sahakaro K., Beraheng S.: Reinforcement of maleated natural rubber by precipitated silica. *Journal of Applied Polymer Science*, **109**, 3839–3848 (2008).
<https://doi.org/10.1002/app.28483>
- [5] Saramolee P., Lopattananon N., Sahakaro K.: Preparation and some properties of modified natural rubber bearing grafted poly(methyl methacrylate) and epoxide groups. *European Polymer Journal*, **56**, 1–10 (2014).
<https://doi.org/10.1016/j.eurpolymj.2014.04.008>
- [6] Krainoi A., Kummerlöwe C., Nakaramontri Y., Vennemann N., Pichaiyut S., Wisunthorn S., Nakason C.: Influence of critical carbon nanotube loading on mechanical and electrical properties of epoxidized natural rubber nanocomposites. *Polymer Testing*, **66**, 122–136 (2018).
<https://doi.org/10.1016/j.polymertesting.2018.01.003>
- [7] Matos C. F., Galembeck F., Zarbin A. J. G.: Multifunctional and environmentally friendly nanocomposites between natural rubber and graphene or graphene oxide. *Carbon*, **78**, 469–479 (2014).
<https://doi.org/10.1016/j.carbon.2014.07.028>
- [8] Nakaramontri Y., Kummerlöwe C., Vennemann N., Wisunthorn S., Pichaiyut S., Nakason C.: Effect of bis(triethoxysilylpropyl) tetrasulfide (TESPT) on properties of carbon nanotubes and conductive carbon black hybrid filler filled natural rubber nanocomposites. *Express Polymer Letters*, **12**, 867–884 (2018).
<https://doi.org/10.3144/expresspolymlett.2018.75>
- [9] Salaeh S., Muensit N., Bomlai P., Nakason C.: Ceramic/natural rubber composites: Influence types of rubber and ceramic materials on curing, mechanical, morphological, and dielectric properties. *Journal of Material Sciences*, **46**, 1723–1731 (2011).
<https://doi.org/10.1007/s10853-010-4990-6>
- [10] Zhang X., Tang Z., Guo B., Zhang L.: Enabling design of advanced elastomer with bioinspired metal–oxygen coordination. *ACS Applied Materials and Interfaces*, **8**, 32520–32527 (2016).
<https://doi.org/10.1021/acsami.6b10881>
- [11] Rippel M. M., Leite C. A. P., Galembeck F.: Elemental mapping in natural rubber latex films by electron energy loss spectroscopy associated with transmission electron microscopy. *Analytical Chemistry*, **74**, 2541–2546 (2002).
<https://doi.org/10.1021/ac0111661>
- [12] Nawamawat K.: Effect of non-rubber components on basic characteristics and physical properties on natural rubber form *Hevea brasiliensis*. Ph.D. dissertation, Mahidol University, Bangkok, Thailand (2008).
- [13] Kurian T., Mathew N. M.: Natural rubber: Production, properties and applications. in ‘Biopolymers: Biomedical and environmental applications’ (eds.: Kalia S., Avérous L.) Scrivener, Salem, 403–436 (2011).
<https://doi.org/10.1002/9781118164792.ch14>
- [14] Gan S-N., Ting K-F.: Effect of treating latex with some metal ions on storage hardening of natural rubber. *Polymer*, **34**, 2142–2147 (1993).
[https://doi.org/10.1016/0032-3861\(93\)90742-s](https://doi.org/10.1016/0032-3861(93)90742-s)
- [15] Hamerton I., Howlin B. J., Jones J. R., Liu S., Barton J. M.: Preparation of metal-aromatic diamine complexes and their influence on the cure of a commercial epoxy resin. *Polymer Bulletin*, **36**, 295–302 (1995).
<https://doi.org/10.1007/bf00319228>
- [16] Mandal S., Simon F., Banerjee S., Tunnicliffe L., Nakason C., Das C., Das M., Naskar K., Wiessner S., Heinrich G., Das A.: Controlled release of metal ion cross-linkers and development of self-healable epoxidized natural rubber. *ACS Applied Polymer Materials*, **3**, 1190–1202 (2021).
<https://doi.org/10.1021/acsapm.1c00039>
- [17] Damampai K., Pichaiyut S., Mandal S., Wießner S., Das A., Nakason C.: Internal polymerization of epoxy group of epoxidized natural rubber by ferric chloride and formation of strong network structure. *Polymers*, **13**, 4145 (2021).
<https://doi.org/10.3390/polym13234145>
- [18] Bořkovec A. B.: Reaction of epoxides with ferric chloride. *Journal of Organic Chemistry*, **23**, 828–830 (1958).
<https://doi.org/10.1021/jo01100a017>
- [19] Ebbesen T. W., Ajayan P. M.: Large-scale synthesis of carbon nanotubes. *Nature*, **358**, 220–222 (1992).
<https://doi.org/10.1038/358220a0>
- [20] Das A., Kasaliwal G. R., Jurk R., Boldt R., Fischer D., Stöckelhuber K. W., Heinrich G.: Rubber composites based on graphene nanoplatelets, expanded graphite, carbon nanotubes and their combination: A comparative study. *Composites Science and Technology*, **72**, 1961–1967 (2012).
<https://doi.org/10.1016/j.compscitech.2012.09.005>
- [21] Mensah B., Kim H. G., Lee J-H., Arepalli S., Nah C.: Carbon nanotube-reinforced elastomeric nanocomposites: A review. *International Journal of Smart and Nano Materials*, **6**, 211–238 (2015).
<https://doi.org/10.1080/19475411.2015.1121632>
- [22] Nakaramontri Y., Kummerlöwe C., Nakason C., Vennemann N.: Effect of modified natural rubber and functionalization of carbon nanotubes on properties of natural rubber composites. *Advanced Materials Research*, **844**, 301–304 (2014).
<https://doi.org/10.4028/www.scientific.net/AMR.844.301>

- [23] Matchawet S., Kaesaman A., Bomlai P., Nakason C.: Effects of multi-walled carbon nanotubes and conductive carbon black on electrical, dielectric, and mechanical properties of epoxidized natural rubber composites. *Polymer Composites*, **38**, 1031–1042 (2015).
<https://doi.org/10.1002/pc.23666>
- [24] Shanmugaraj A. M., Ryu S. H.: Influence of aminosilane-functionalized carbon nanotubes on the rheometric, mechanical, electrical and thermal degradation properties of epoxidized natural rubber nanocomposites. *Polymer International*, **62**, 1433–1441 (2013).
<https://doi.org/10.1002/pi.4437>
- [25] Nakaramontri Y., Nakason C., Kummerlöwe C., Vennemann N.: Influence of modified natural rubber on properties of natural rubber-carbon nanotube composites. *Rubber Chemistry and Technology*, **88**, 199–218 (2015).
<https://doi.org/10.5254/rct.14.85949>
- [26] Ismail H., Salleh S. Z., Ahmad Z.: Fatigue and hysteresis behavior of halloysite nanotubes-filled natural rubber (SMR L and ENR 50) nanocomposites. *Journal of Applied Polymer Science*, **127**, 3047–3052 (2012).
<https://doi.org/10.1002/app.37587>
- [27] Nakaramontri Y., Nakason C., Kummerlöwe C., Vennemann N.: Effects of *in-situ* functionalization of carbon nanotubes with bis(triethoxysilylpropyl) tetrasulfide (TESPT) and 3-aminopropyltriethoxysilane (APTES) on properties of epoxidized natural rubber-carbon nanotube composites. *Polymer Engineering and Science*, **55**, 2500–2510 (2015).
<https://doi.org/10.1002/pen.24140>
- [28] Subramaniam K., Das A., Heinrich G.: Development of conducting polychloroprene rubber using imidazolium based ionic liquid modified multi-walled carbon nanotubes. *Composites Science and Technology*, **71**, 1441–1449 (2011).
<https://doi.org/10.1016/j.compscitech.2011.05.018>
- [29] Das A., Stöckelhuber K. W., Jurk R., Fritzsche J., Klüppel M., Heinrich G.: Coupling activity of ionic liquids between diene elastomers and multi-walled carbon nanotubes. *Carbon*, **47**, 3313–3321 (2009).
<https://doi.org/10.1016/j.carbon.2009.07.052>
- [30] Krainoi A., Kummerlöwe C., Nakaramontri Y., Wisunthorn S., Vennemann N., Pichaiyut S., Kiatkamjornwong S., Nakason C.: Influence of carbon nanotube and ionic liquid on properties of natural rubber nanocomposites. *Express Polymer Letters*, **13**, 327–348 (2019).
<https://doi.org/10.3144/expresspolymlett.2019.28>
- [31] Payne A. R., Whittaker R. E.: Low strain dynamic properties of filled rubbers. *Rubber Chemistry and Technology*, **44**, 440–478 (1971).
<https://doi.org/10.5254/1.3547375>
- [32] Nakaramontri Y., Kummerlöwe C., Nakason C., Vennemann N.: The effect of surface functionalization of carbon nanotubes on properties of natural rubber-carbon nanotube composites. *Polymer Composites*, **36**, 2113–2122 (2014).
<https://doi.org/10.1002/pc.23122>
- [33] Du F., Fischer J., Winey K.: Coagulation method for preparing single-walled carbon nanotube/poly(methyl methacrylate) composites and their modulus, electrical conductivity, and thermal stability. *Polymer Science: Part B*, **41**, 3333–3338 (2003).
<https://doi.org/10.1002/polb.10701>
- [34] Flory P. J., Rehner J. R.: Statistical mechanics of cross-linked polymer networks II. Swelling. *Journal of Chemical Physics*, **11**, 521–526 (1943).
<https://doi.org/10.1063/1.1723792>
- [35] Hamzah R., Abu Bakar M., Khairuddean M., Mohammed I. A., Adnan R.: A structural study of epoxidized natural rubber (ENR-50) and its cyclic dithiocarbonate derivative using NMR spectroscopy techniques. *Molecules*, **17**, 10974–10993 (2012).
<https://doi.org/10.3390/molecules170910974>
- [36] Biju C. S.: Properties of α -Fe₂O₃/graphene nanohybrid synthesized by a simple hydrothermal/solution mixing method. *Nano-Structures and Nano-Objects*, **13**, 44–50 (2018).
<https://doi.org/10.1016/j.nanoso.2017.12.005>
- [37] Coates J.: Interpretation of infrared spectra, A practical approach. in ‘Encyclopedia of analytical chemistry’ (ed.: Meyers R. A.) Elsevier, Chichester, 1–23 (2006).
<https://doi.org/10.1002/9780470027318.a5606>
- [38] Das A., Stöckelhuber K. W., Jurk R., Fritzsche J., Klüppel M., Heinrich G.: Coupling activity of ionic liquids between diene elastomers and multi-walled carbon nanotubes. *Carbon*, **47**, 3313–3321 (2009).
<https://doi.org/10.1016/j.carbon.2009.07.052>
- [39] Payne A. R.: Effect of dispersion on dynamic properties of filler-loaded rubbers. *Rubber Chemistry and Technology*, **39**, 365–374 (1966).
<https://doi.org/10.5254/1.3544848>
- [40] Kołodziejczak-Radzimska A., Markiewicz E., Jesionowski T.: Structural characterisation of ZnO particles obtained by the emulsion precipitation method. *Journal of Nanomaterials*, **2012**, 656353 (2012).
<https://doi.org/10.1155/2012/656353>
- [41] Subramaniam K., Das A., Stöckelhuber K. W., Heinrich G.: Elastomer composites based on carbon nanotubes and ionic liquid. *Rubber Chemistry and Technology*, **86**, 367–400 (2013).
<https://doi.org/10.5254/rct.13.86984>
- [42] Fröhlich J., Niedermeier W., Luginsland H-D.: The effect of filler–filler and filler–elastomer interaction on rubber reinforcement. *Composites Part A: Applied Science and Manufacturing*, **36**, 449–460 (2005).
<https://doi.org/10.1016/j.compositesa.2004.10.004>
- [43] Salaeh S., Boiteux G., Cassagnau P., Nakason C.: Flexible 0–3 ceramic-polymer composites of barium titanate and epoxidized natural rubber. *International Journal of Applied Ceramic Technology*, **12**, 106–115 (2015).
<https://doi.org/10.1111/ijac.12129>